Amita Shukla-Dave, PhD
Hedvig Hricak, MD, PhD
Steven C. Eberhardt, MD
Semra Olgac, MD
Manickam Muruganandham, PhD
Peter T. Scardino, MD
Victor E. Reuter, MD
Jason A. Koutcher, MD, PhD
Kristen L. Zakian, PhD

Index terms:
Magnetic resonance (MR), spectroscopy, 844.12145
Prostate, MR, 844.121411
Prostate neoplasms, MR, 844.121411, 844.12145
Prostatitis, 844.214

Published online
10.1148/radiol.2313031391
Radiology 2004; 231:717–724

Abbreviations:
BASING = band-selective inversion with gradient dephasing
PRESS = point-resolved spectroscopy
SI = signal intensity

[1] From the Departments of Radiology (A.S.D., H.H., S.C.E., J.A.K., K.L.Z.), Medical Physics (A.S.D., M.M., J.A.K., K.L.Z.), Pathology (S.O., V.E.R.), Medicine (J.A.K.), and Urology (P.T.S.), Memorial Sloan-Kettering Cancer Center, 1275 York Ave, New York, NY 10021. Received August 29, 2003; revision requested October 21; revision received December 15; accepted January 13, 2004. Supported by National Institutes of Health grant RO1 CA76423. **Address correspondence to** A.S.D. (e-mail: *davea@mskcc.org*).

Author contributions:
Guarantors of integrity of entire study, A.S.D., H.H., K.L.Z.; study concepts, A.S.D., K.L.Z., H.H., S.C.E., P.T.S., V.E.R., J.A.K.; study design, A.S.D., K.L.Z., H.H., P.T.S., J.A.K., V.E.R.; literature research, A.S.D.; clinical studies, V.E.R., S.O., P.T.S., H.H., S.C.E., K.L.Z., A.S.D., M.M.; data acquisition, A.S.D., M.M.; data analysis/interpretation, A.S.D., K.L.Z., S.C.E., H.H.; manuscript preparation, A.S.D., K.L.Z., H.H., S.C.E., V.E.R., J.A.K.; manuscript definition of intellectual content, A.S.D., K.L.Z., H.H.; manuscript editing, H.H., S.C.E., J.A.K., V.E.R., P.T.S., M.M., S.O., K.L.Z.; manuscript revision/review, all authors; manuscript final version approval, H.H., J.A.K., S.C.E., K.L.Z., A.S.D.

Chronic Prostatitis: MR Imaging and ^{1}H MR Spectroscopic Imaging Findings—Initial Observations[1]

PURPOSE: To determine whether chronic prostatitis affects three-dimensional proton magnetic resonance (MR) spectroscopic imaging in evaluation of disease in the peripheral zone.

MATERIALS AND METHODS: Combined MR imaging and three-dimensional MR spectroscopic imaging data were examined retrospectively in 12 patients with radical prostatectomy specimens that contained regions of chronic prostatitis larger than 6 mm in the peripheral zone. The 6-mm restriction was based on MR spectroscopic imaging spatial resolution of 6.25 mm. Transverse T2-weighted MR images were reviewed for changes in signal intensity (SI): normal, suspicious for cancer (nodular focal low SI), or indeterminate (focal low SI that was not nodular or contour deforming or diffuse low SI). At MR spectroscopic imaging, proton spectra were considered suspicious for cancer if the ratio of choline plus creatine to citrate was more than 2 SDs above normal mean peripheral zone values.

RESULTS: In the 12 patients, mean pretreatment prostate-specific antigen level was 5.77 ± 2.07 (SD), and median biopsy Gleason score for the gland was 6. At MR imaging in the area of histopathologically confirmed chronic prostatitis, seven of 12 patients had focal low SI that was not nodular (contour deforming) over a region in and around the pathologically defined focus of chronic prostatitis. MR imaging in one patient showed diffuse low SI that correlated with a diffuse area of chronic prostatitis at pathologic examination. MR imaging in another patient showed nodular focal low SI that was suspicious for cancer and corresponded to a focus of chronic prostatitis at pathologic examination. The remaining three patients had no MR imaging abnormality in the region of chronic prostatitis. In the pathologically identified regions of chronic prostatitis, MR spectroscopic imaging data in nine of 12 patients demonstrated elevated choline peak and reduced or no citrate, findings that mimic those of cancer. In two patients, the spectra were normal, and in the remaining patient, the spectra were nondiagnostic.

CONCLUSION: At MR spectroscopic imaging, pathologically confirmed chronic prostatitis may demonstrate metabolic abnormality that leads to false-positive diagnosis of cancer. The most common MR imaging finding in chronic prostatitis was focal low SI that was not specific for cancer. In one patient, the MR imaging diagnosis of cancer could not be excluded.

Combined magnetic resonance (MR) imaging and hydrogen 1 MR spectroscopic imaging may become an important tool in the detection and staging of prostate cancer (1–4). MR images, particularly high-spatial-resolution endorectal T2-weighted MR images, demonstrate high signal intensity (SI) in healthy peripheral zone tissue and low SI in cancerous areas. However, certain benign conditions including prostatitis, benign prostatic hyper-

plasia, fibrosis, intraglandular dysplasia, and glandular atrophy may also have low SI, a finding that mimics that of cancer (5–7). The ^{1}H MR spectroscopic imaging findings add specificity to the MR imaging findings in cancer detection and localization, and in the prostate gland, they expand the diagnostic assessment of prostate cancer by depicting cellular metabolites. Prostate cancer can be distinguished from healthy peripheral zone tissue on the basis of the ratio of choline plus creatine to citrate (3,8). The reported sensitivity and specificity, respectively, for cancer localization within the peripheral zone of the prostate gland for MR imaging are 67% and 69% and those for MR spectroscopic imaging are 76% and 57% (9). Combined results from MR imaging and MR spectroscopic imaging yield sensitivity of 56% and specificity of 82% (10). The purpose of our study was to determine whether chronic prostatitis affects three-dimensional proton MR spectroscopic imaging in the evaluation of disease in the peripheral zone.

MATERIALS AND METHODS

Subjects

This retrospective study included 101 patients with prostate cancer who underwent preoperative MR imaging and three-dimensional MR spectroscopic imaging in the prostate between February 2000 and February 2003. The patients underwent radical prostatectomy, and whole-mount step-section pathologic findings were available. The institutional committee on human research approved the study, and written informed consent was obtained from all patients. These patients are a subset of an ongoing institutional review board–approved National Institutes of Health study to investigate the value of MR imaging and MR spectroscopic imaging in prostate cancer in patients who provide informed consent.

At histopathologic evaluation, 30 of the 101 patients also had a diagnosis of chronic prostatitis on the official pathology report. The pathologists (V.E.R., S.O.) reevaluated the 30 step-section pathologic maps and detailed areas of cancer, chronic prostatitis, and normal tissue. Among the 30 patients, 12 had chronic prostatitis in the transition zone and were excluded from further analysis. In 18 patients, chronic prostatitis was present in the peripheral zone. The study inclusion criteria also required that the nonneoplastic tissue diagnosed as chronic prostatitis in the pathology report should be larger than 6 mm in the in-plane diameter because the spatial resolution of the MR spectroscopic imaging voxel was 6.25 mm. In six of the 18 patients, the area of chronic prostatitis was smaller than 6 mm in largest diameter; this finding precluded comparison of MR spectroscopic imaging and histopathologic findings. Thus, our retrospective study included the 12 patients with chronic prostatitis in the peripheral zone (age range, 50–67 years; mean, 56.8 years ± 5.3 [SD]).

MR Imaging Data Acquisition and Processing

MR imaging and MR spectroscopic imaging data were acquired with a 1.5-T MR system (Signa Horizon; GE Medical Systems, Milwaukee, Wis) with software developed at the University of California at San Francisco (11–14). Each study consisted of MR imaging with a pelvic phased array and expandable endorectal coil. Sagittal fast spin-echo localization images were obtained to check the endorectal coil position and to define the subsequent MR imaging sequences. Transverse T1-weighted spin-echo MR images (repetition time msec/echo time msec of 700/12, field of view of 24, section thickness of 5.0 mm, intersection gap of 1.0 mm, matrix of 256 × 192, and two signals acquired) were obtained and then T2-weighted fast spin-echo MR images (4,000/102, field of view of 14, section thickness of 3.0 mm, no intersection gap, matrix of 256 × 192, and four signals acquired) were obtained in the transverse and coronal planes through the prostate and seminal vesicles. We used the MR imaging system software (PACC; GE Medical Systems) to correct the transverse T1- and T2-weighted MR images for the reception profile of the endorectal and external pelvic phased-array coils. The total time for setup and acquisition was approximately 30 minutes. MR imaging was followed by MR spectroscopic imaging with point-resolved spectroscopy (PRESS) voxel excitation (15), and band-selective inversion with gradient dephasing (BASING) water and lipid suppression (11). The 17-minute MR spectroscopic imaging acquisition resulted in a voxel array with in-plane resolution of 6.25 mm and the SI dimension zero filled to 16 sections (3.1-mm resolution). Data were processed with a workstation (Ultra 10; Sun Microsystems, Mountain View, Calif). Processing included 2-Hz Lorentzian apodization in the time domain, four-dimensional Fourier transform, and automated frequency, phase, and baseline correction of each voxel (14). Peak areas were calculated by means of numeric integration. For all voxels, the ratio of choline plus creatine to citrate was calculated.

MR Data Interpretation: Evaluation of SI

Manual matching between MR images and step-section pathololgic examination was performed by one radiologist (S.C.E.) with use of anatomic landmarks such as individual adenomatous nodules in the transition zone or the ejaculatory ducts and verumontanum or distal urethra. Two radiologists (H.H., S.C.E.) were involved in the study. One of the two radiologists (S.C.E.), with 4 years of experience in interpreting endorectal MR images of the prostate, matched the findings in whole-mount step-section pathologic specimens with those on the most closely corresponding transverse T2-weighted MR images and marked the area of chronic prostatitis on the MR images. In a separate session, the other radiologist (H.H.), with more than 10 years of experience in the interpretation of endorectal MR images of the prostate, examined the indicated regions of chronic prostatitis in the peripheral zone on the T2-weighted MR images and categorized the SI in the chronic prostatitis region as follows: *(a)* normal, homogeneous high SI; *(b)* suspicious for cancer, focal nodular mass demonstrates homogeneous low SI (SI lower than that of adjacent normal peripheral zone); and *(c)* indeterminate, which was further divided into focal low-SI area that was not nodular (contour deforming) and diffuse low SI present in entire half or more of the peripheral zone with no mass effect. The criteria for MR image analysis were based on previously reported MR imaging findings (6,16,17) and supplemented with the personal experience of the radiologist.

Analysis of MR Spectroscopic Imaging Data

In each MR spectroscopic imaging data set, voxels were assessed for the signal-to-noise ratio. MR spectroscopic imaging data sets had approximately 10%–13% of peripheral zone voxels that were unusable because of artifact due to lipid contamination in the excitation volume or because they included tissue from the urethra and ejaculatory ducts (8). Spectral voxels with signal-to-noise ratios for choline and citrate peaks of less than 5.0 were considered to have no metabolites present and were nondiagnostic. Two of

MR Imaging and MR Spectroscopic Imaging Findings in 12 Patients with Chronic Prostatitis Identified at Step-Section Pathologic Examination

Patient No./ Age (y)	Gleason Score	PSA Level (ng/mL)*	Clinical Stage	MR Spectroscopic Imaging: No. of Abnormal Voxels	MR Spectroscopic Imaging: Grade†	MR Spectroscopic Imaging: No. of Clusters	MR Imaging Findings
1/59	6	3.3	T1c	0	Nondiagnostic	0	Normal
2/51	6	6.2	T1c	2	2 IG	1	Normal
3/67	6	7.0	T2a	1	1 IG	1	Focal low T2 SI‡
4/50	6	4.5	T1c	1	1 IG	1	Focal low T2 SI‡
5/54	6	4.6	T2a	2	1 LG, 1 IG	1	Focal low T2 SI‡
6/52	6	3.9	T2a	15	2 LG, 9 IG, 4 HG	2	1 normal, 1 nodular focal low T2 SI
7/58	6	5.7	T1c	0	Healthy	0	Focal low T2 SI‡
8/61	7	4.7	T2a	3	3 IG	1	Focal low T2 SI‡
9/59	6	9.8	T2a	0	Healthy	0	Normal
10/63	6	9.3	T2a	6	2 LG, 4 IG	1	Focal low T2 SI‡
11/57	6	4.0	T1c	20	2 LG, 6 IG, 12 HG	1§	Diffuse low T2 SI
12/51	7	6.2	T2b	8	1 LG, 6 IG, 1 HG	2	Focal low T2 SI‡

* PSA = prostate-specific antigen.
† Diagnostic voxels were classified as healthy or cancer: LG = low grade (ratio of choline plus creatine to citrate of 0.5–0.6, IG = intermediate grade (ratio of 0.7–3.0), HG = high grade (ratio greater than 3.0).
‡ Not nodular (contour deforming).
§ With large number of contiguous abnormal voxels. Patient had histopathologically proved diffuse chronic prostatitis.

the 12 patients had nondiagnostic voxels (16 of 77 voxels [21%]) in the area of chronic prostatitis, with one voxel in one patient and 15 in the other. In the usable MR spectroscopic imaging data set, a ratio of choline plus creatine to citrate of more than 0.5 (2 SDs more than normal mean peripheral zone values) was considered suspicious for cancer (3).

Diagnostic voxels were classified as healthy or cancerous: low-grade cancer (ratio of choline plus creatine to citrate of 0.5–0.6), intermediate-grade cancer (ratio of 0.7–3.0), or high-grade cancer (ratio greater than 3.0). This classification was based on the observation that reduced citrate and elevated choline levels correlate with tumor aggressiveness (3, 18–20). Two or more contiguous abnormal voxels were grouped as a cluster. A cluster may represent either focal or diffuse (one cluster with a large number of contiguous abnormal voxels) metabolic abnormality. In addition to metabolite ratios, abnormal voxels in which only choline was detectable were also assessed (20).

Pathologic Findings

After radical prostatectomy, each prostate specimen was coated with India ink and fixed in 10% buffered formaldehyde. The distal 5-mm portion of the apex was amputated and coned. The remainder of the gland was serially sectioned at 3–4-mm intervals from base to apex. All prostate pathologic step sections were submitted for paraffin embedding as whole mounts and labeled according to location. The presence and extent of cancer, chronic prostatitis, and normal tissue for each section were determined by an experienced pathologist. We hoped to limit interobserver variability; therefore, the slides were reviewed by two pathologists (V.E.R., with 21 years of experience with prostate disease; S.O., with 4 years of experience) in consensus about the area of chronic prostatitis. Chronic prostatitis, an inflammatory condition of the prostate, was determined in whole-mount pathology step sections on the basis of the presence of a dense collection of chronic inflammatory cells, particularly lymphocytes, located in the prostatic stroma and surrounding prostatic ducts and acini. Chronic prostatitis lesions were categorized as either focal or diffuse (ie, extending from the base to the apex in entire half or more of the peripheral zone). The focality in terms of multiple foci or one focus and the largest in-plane diameter of the foci of chronic prostatitis were measured and recorded in each gland.

RESULTS

All 12 patients evaluated in this study had a histopathologic diagnosis of cancer and chronic prostatitis. Details of the clinical, MR imaging, and MR spectroscopic imaging information are given in the Table. Of the 12 patients with chronic prostatitis (6 mm or more in diameter) in the peripheral zone, the mean pretreatment prostate-specific antigen level was 5.77 ± 2.07 and the median Gleason score for the gland at biopsy was 6. In 11 of the 12 patients, chronic prostatitis seen in pathologic step sections was found to be multifocal, while in the remaining patient, there was one diffuse area of chronic prostatitis, which extended from the base to the apex in the right half of the gland. In patients with multifocal chronic prostatitis, only those foci that met the inclusion criteria for largest diameter were studied. The largest diameter of the focus ranged from 6 to 40 mm (mean, 12 mm ± 2.7 [standard error of the mean]). In the region of histopathologically confirmed chronic prostatitis, the MR images in seven of the 12 patients (58%) had focal low SI that was not nodular (contour deforming). This focal low SI encompassed but also extended beyond the pathologically defined focus of chronic prostatitis. In one of the 12 patients, the MR image showed diffuse low SI that correlated with a diffuse area of chronic prostatitis at pathologic examination. In one patient, the MR image showed nodular focal low SI that was suspicious for cancer and corresponded to a focus of chronic prostatitis at pathologic examination. In the remaining three patients, no imaging abnormality was seen in the pathologically defined region of chronic prostatitis.

The MR spectroscopic imaging data from the 12 patients had a combined total of 77 voxels in the area of chronic prostatitis. In two patients, three voxels had normal spectra in the region of chronic prostatitis. One patient had one voxel in the chronic prostatitis region, which was nondiagnostic. In the remain-

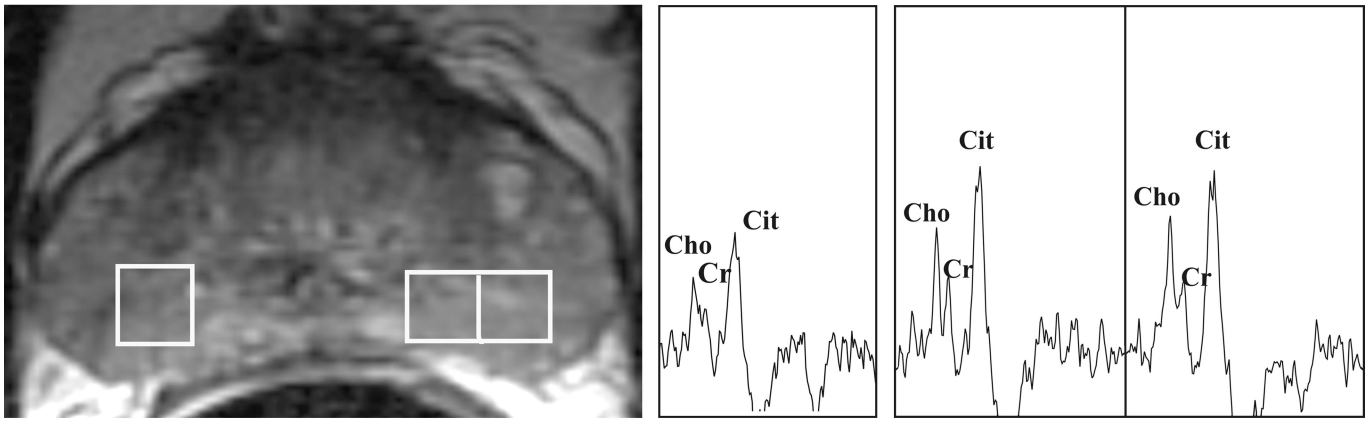

a. b. c.

d.

Figure 1. MR imaging, MR spectroscopic imaging, and pathologic data in a 54-year-old patient with prostate cancer (clinical stage T2a, Gleason score of 6, and prostate-specific antigen level of 4.6 ng/mL). **(a)** Transverse T2-weighted fast spin-echo MR image (section position, I49.81) (4,000/102, 14-mm field of view, 3.0-mm section thickness, no intersection gap, 256 × 192 matrix, and four signals acquired) shows three voxels of interest marked with white lines. **(b, c)** MR spectra were obtained with PRESS volume excitation with BASING water and lipid suppression (1,000/130, 16 × 8 × 8 chemical shift imaging, 100 × 50 × 50-mm field of view, 6.25-mm resolution, one signal acquired, and 17-minute imaging time). Spectra of voxels of interest exhibit elevated choline and reduced citrate peaks. **(d)** Step-section pathologic map corresponds to MR image in **a**, with prostate cancer outlined in black lines in left and right peripheral zones. Voxels of interest in **a** are cancer, as confirmed at histopathologic examination *(Fig 1 continues).*

ing nine patients, MR spectroscopic imaging demonstrated an elevated choline peak and reduced or no citrate, mimicking cancer in voxels corresponding to the area of histopathologically confirmed chronic prostatitis. Of these nine patients with 58 false-positive voxels, seven had clustered false-positive voxels (two or more contiguous abnormal voxels) and two had only one abnormal voxel that corresponded to each focus of chronic prostatitis (Table). Of the seven patients with clusters of abnormal voxels, six had focal MR spectroscopic imaging abnormality that corresponded to focal pathologically proved chronic prostatitis. The seventh patient had a large number of abnormal voxels (20) that were contiguous and therefore technically defined as a cluster. This patient had diffuse histopathologically confirmed chronic prostatitis.

Of the 58 false-positive voxels, eight voxels indicated low-grade cancer (mean choline plus creatine to citrate ratio, 0.6 ± 0.0), 33 indicated intermediate-grade cancer (mean ratio, 1.2 ± 0.1), and 17 indicated high-grade cancer (mean ratio, 7.9 ± 0.8). Of the 17 voxels that indicated high-grade cancer, 10 had elevated choline with no citrate. Eighty-six percent of the 58 false-positive voxels were in the intermediate-grade (n = 33) or high-grade (n = 17) groups.

These findings are illustrated in Figures 1 and 2, which contain MR images with corresponding three-dimensional MR spectroscopic imaging and histopathologic photomicrographs. Figure 1 shows data from a patient with chronic prostatitis and cancer in different sextant locations; the spectral metabolic patterns in cancer and chronic prostatitis indicate intermediate-grade disease. In Figure 2, data are shown from a patient with severe chronic prostatitis and a small focus of cancer at step-section pathologic examination. The MR spectroscopic imaging data show 35 voxels that correspond to chronic prostatitis, of which 20 were diagnostic and 15 were nondiagnostic. The abnormal metabolic pattern in the spectral data depicts minimal or no citrate and elevated choline; these findings mimic those of cancer.

DISCUSSION

Detection of prostatitis with imaging modalities such as transrectal ultrasonography (21–25) and MR imaging (26–30) remains a challenge. Ikonen et al (7) assessed the accuracy of MR imaging in the differentiation of cancer from other prostatic disorders, such as benign prostatic hyperplasia, acute bacterial prostatitis, and chronic bacterial prostatitis. In their study, accuracy of diagnosis of cancer was high, but differentiation of bacterial prostatitis from cancer was difficult because the former showed some features similar to those of the latter. Without the integration of clinical data, MR imaging was insensitive in the differentiation of cancer from other prostatic disorders. In a similar study, Engelhard et al (6) attempted to differentiate benign prostatic lesions from cancer with MR imaging. They observed low SI ratios in areas of biopsy-proved chronic prostatitis. This result is in agreement with findings in the present study. The difference between their study and ours is that they used prostate biopsy as the reference standard, while we used step-section pathologic examination. In the present study, we defined chronic prostatitis pathologically, which may not correlate with clinical chronic prostatitis. It is recognized that in the diagnosis of chronic prostatitis, biopsy has limited sensitivity and specificity (31). In the present study, MR imaging demonstrated indeterminate focal low SI that was not nodular (contour deforming) in 58% of chronic prostatitis lesions that were greater than 6 mm in largest diameter. In one patient, the diagnosis of cancer at MR imaging

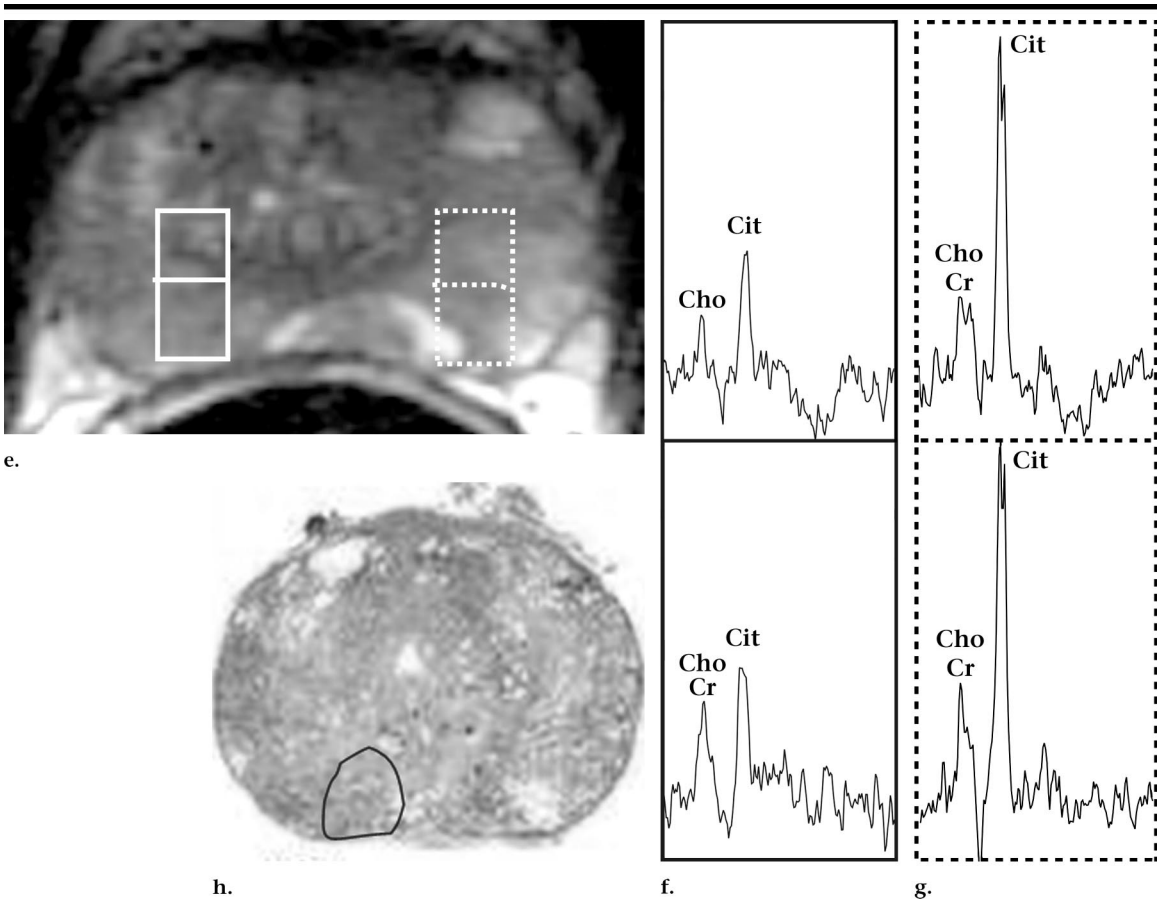

Figure 1 *(continued).* **(e)** Transverse T2-weighted MR image (section position, I59.19) shows two regions of interest, one marked with solid lines and the other marked with dashed lines. **(f)** MR spectra from voxels marked with solid lines exhibits elevated choline and reduced citrate. **(g)** MR spectra from voxels marked with dashed lines exhibits healthy peripheral zone, elevated citrate, and equal low peaks of choline and creatine. **(h)** Step-section pathologic map corresponds to MR image in **e**, with chronic prostatitis outlined with black line in right peripheral zone. Findings mimicked those of cancer.

could not be excluded in the area of chronic prostatitis. We emphasize that the present study was not intended to assess the sensitivity of MR imaging in the detection of chronic prostatitis or cancer but simply to assess the relationship between MR imaging and MR spectroscopic imaging characteristics and pathologic findings.

Current MR spectroscopic imaging technology allows acquisition of high-spatial-resolution (0.24 cm^3) proton spectra from the entire prostate in a clinically reasonable time. High levels of citrate and low levels of creatine and choline are the metabolic signature in a proton spectrum for healthy prostatic tissue (2,3,32–36). It is known that prostatic glandular cells demonstrate unique mitochondrial and cytosolic processes with high production of citrate (37,38). Cancer, however, is identified on the basis of elevated choline and a ratio of choline plus creatine to citrate of 0.5 or more when PRESS excitation with BASING water and lipid suppression is applied (3,8,18).

In their prospective study, Van Dorsten et al (39) found that chronic prostatitis does not necessarily result in abnormal metabolic ratios. This was also shown in two of our 12 patients with histopathologically confirmed chronic prostatitis. Findings mimicked those of cancer in nine patients, and the spectra were nondiagnostic in one patient. Both our study and theirs involved small numbers of patients, but the standards of reference were different. In the present study, we used volumetric MR spectroscopic imaging data and step-section pathologic findings as the reference standard. In their study, patients with clinical symptoms suggestive of prostatitis syndrome underwent MR imaging. The radiologist localized the potential inflammatory lesion, and single-section two-dimensional ^1H MR spectroscopic imaging was performed at that position. In the present study, choline was elevated in nine of 12 patients with histopathologically confirmed chronic prostatitis, and 86% of the voxels indicated intermediate- or high-grade disease. This metabolic pattern mimics that of cancer, which results in false-positive findings.

Findings in histologic studies (40,41) provide a basis for the metabolic alterations observed. The lumina may become compressed with inflammatory cells, which results in a reduction in the citrate level (42–44). The reduction in citrate is seen in the proton spectra in cases of cancer and chronic prostatitis.

Our study has several limitations. We studied a cohort of patients with the diagnosis of chronic prostatitis in the surgical pathology reports (ie, we studied patients with pathologically proved chronic prostatitis). We did not select patients on the basis of clinical chronic prostatitis. Consequently, we may have missed patients for the study. The

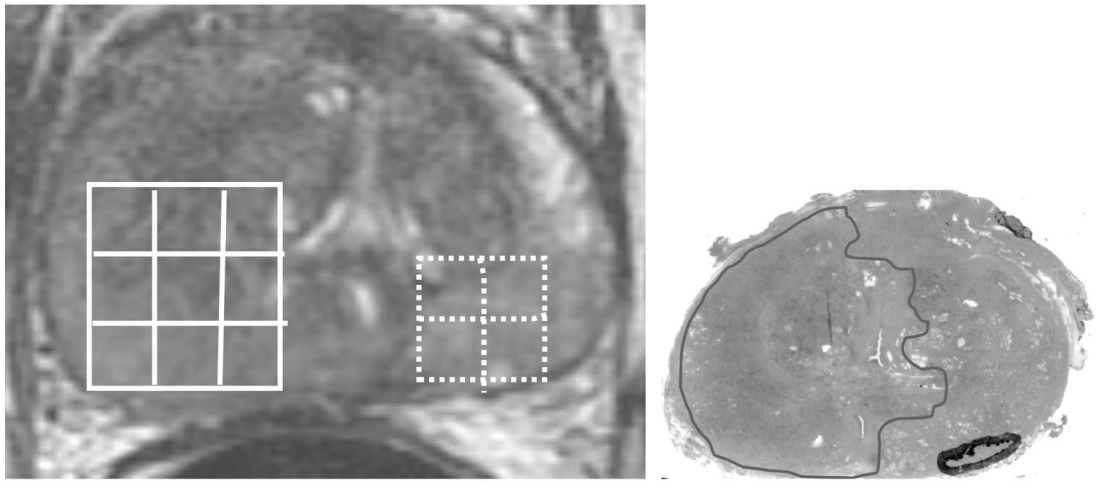

a.

d.

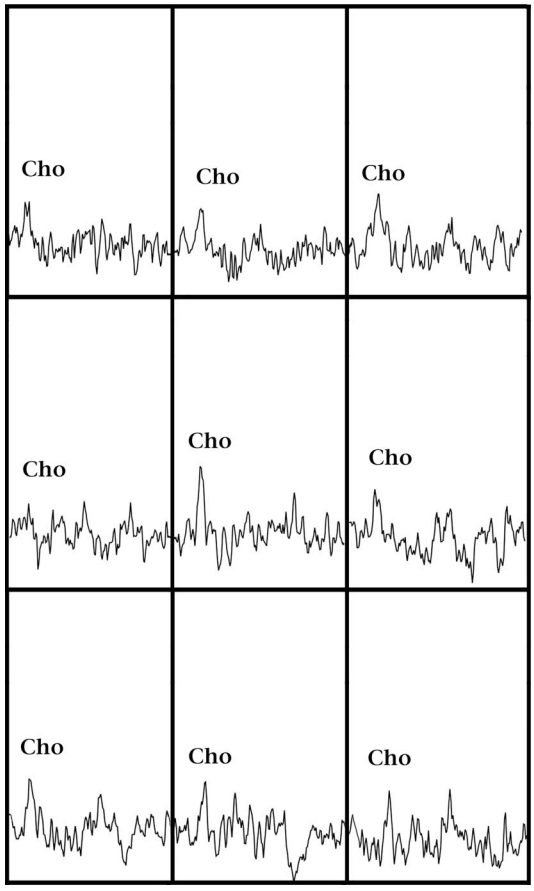

b.

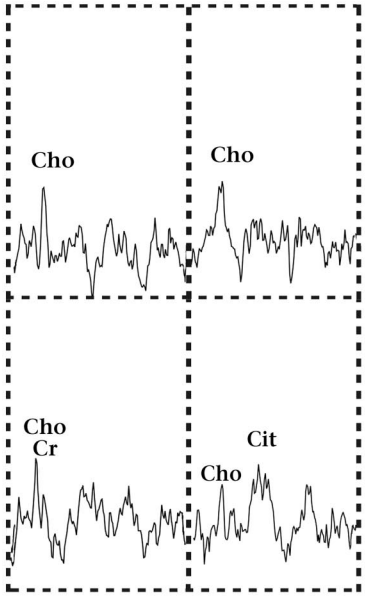

c.

Figure 2. MR imaging, MR spectroscopic imaging, and pathologic data in a 57-year-old patient with prostate cancer (clinical stage T1c, Gleason score of 6, and prostate-specific antigen level of 4.0 ng/mL). This patient had a clinical history of chronic prostatitis, and histopathologic findings confirmed severe chronic prostatitis and focal cancer. **(a)** Transverse T2-weighted MR image (4,000/102, 14-mm field of view, 3.0-mm section thickness, no intersection gap, 256 × 192 matrix, and four signals acquired) shows two regions of interest, one marked with solid lines and the other marked with dashed lines. Regions of interest exhibit abnormal diffuse low SI. **(b)** MR spectra were obtained with PRESS volume excitation with BASING water and lipid suppression (1,000/130, 16 × 8 × 8 chemical shift imaging, 100 × 50 × 50-mm field of view, 6.25-mm resolution, one signal acquired, and 17-minute imaging time). Voxels marked with solid lines in **a** have MR spectral pattern of elevated choline and no citrate. These findings mimic those of cancer. **(c)** Voxels marked with dashed line in **a** have MR spectral pattern consistent with cancer. **(d)** Step-section pathologic map corresponds to MR image in **a**, with chronic prostatitis marked with thin line in right half of gland and cancer marked with thick line in left peripheral zone. Spectral findings at MR spectroscopic imaging resulted in overestimation of voxels with cancerlike pattern and caused false-positive findings.

present study also had some technical limitations because we did not include patients with chronic prostatitis in the transition zone because the criteria for diagnosis of transition zone cancer are not yet fully established. Only chronic prostatitis lesions larger than 6 mm in diameter were studied because of limits on spatial resolution. Finally, the low number of patients prevents this study from providing a definitive assessment of the percentage of MR spectroscopic imaging false-positive findings that can be expected in a population as a result of the presence of chronic prostatitis.

Results in the present study show that in vivo prostate metabolism may be altered by inflammation, which results in false-positive interpretations of MR spectroscopic imaging data. A metabolic pattern in areas of inflammation that is interpreted as compatible with high-grade malignant lesions can lead to overly aggressive surgical planning and, possibly, increased morbidity. Thus, findings at MR spectroscopic imaging, as with those from all other clinical tests, must be interpreted critically and in conjunction with other available clinical data.

In summary, in nine of 12 patients, the finding of chronic prostatitis at histopathologic examination correlated with metabolic abnormality suggestive of prostate cancer at MR spectroscopic imaging. Metabolic abnormalities from the regions of chronic prostatitis appeared similar to those for low-, intermediate-, and high-grade cancer. At MR imaging, chronic prostatitis most commonly demonstrated focal low SI that was not specific for cancer. In one patient, however, the diagnosis of cancer could not be excluded.

Acknowledgment: The authors thank Ada Muellner, BA, for editorial assistance.

References

1. Coakley FV, Kurhanewicz J, Lu Y, et al. Prostate cancer tumor volume: measurement with endorectal MR and MR spectroscopic imaging. Radiology 2002; 223: 91–97.
2. Heerschap A, Jager GJ, van der Graaf M, Barentsz JO, Ruijs SH. Proton MR spectroscopy of the normal human prostate with an endorectal coil and a double spin-echo pulse sequence. Magn Reson Med 1997; 37:204–213.
3. Kurhanewicz J, Vigneron DB, Hricak H, Narayan P, Carroll P, Nelson SJ. Three-dimensional H-1 MR spectroscopic imaging of the in situ human prostate with high (0.24–0.7-cm^3) spatial resolution. Radiology 1996; 198:795–805.
4. Schiebler ML, Schnall MD, Pollack HM, et al. Current role of MR imaging in the staging of adenocarcinoma of the prostate. Radiology 1993; 189:339–352.
5. Naik KS, Carey BM. The transrectal ultrasound and MRI appearances of granulomatous prostatitis and its differentiation from carcinoma. Clin Radiol 1999; 54: 173–175.
6. Engelhard K, Hollenbach HP, Deimling M, Kreckel M, Riedl C. Combination of signal intensity measurements of lesions in the peripheral zone of prostate with MRI and serum PSA level for differentiating benign disease from prostate cancer. Eur Radiol 2000; 10:1947–1953.
7. Ikonen S, Kivisaari L, Tervahartiala P, Vehmas T, Taari K, Rannikko S. Prostatic MR imaging: accuracy in differentiating cancer from other prostatic disorders. Acta Radiol 2001; 42:348–354.
8. Kurhanewicz J, Vigneron DB, Males RG, Swanson MG, Yu KK, Hricak H. The prostate: MR imaging and spectroscopy—resent and future. Radiol Clin North Am 2000; 38:115–138.
9. Wefer AE, Hricak H, Vigneron DB, et al. Sextant localization of prostate cancer: comparison of sextant biopsy, magnetic resonance imaging and magnetic resonance spectroscopic imaging with step section histology. J Urol 2000; 164:400–404.
10. Scheidler J, Hricak H, Vigneron DB, et al. Prostate cancer: localization with three-dimensional proton MR spectroscopic imaging—clinicopathologic study. Radiology 1999; 213:473–480.
11. Star-Lack J, Nelson SJ, Kurhanewicz J, Huang LR, Vigneron DB. Improved water and lipid suppression for 3D PRESS CSI using RF band selective inversion with gradient dephasing (BASING). Magn Reson Med 1997; 38:311–321.
12. Moyher SE, Vigneron DB, Nelson SJ. Surface coil MR imaging of the human brain with an analytic reception profile correction. J Magn Reson Imaging 1995; 5:139–144.
13. Vigneron DB, Nelson SJ, Moyher S, Kelley D, Kurhanewicz J, Hricak H. An analytical correction of MR images obtained with endorectal or surface coils. J Magn Reson Imaging 1993; 3:142–145.
14. Nelson SJ, Day MR, Carvajal L. Methods for analysis of serial volume MRI and ^{1}H MRS data for the assessment of response to therapy in patients with brain tumors (abstr). In: Proceedings of the 2nd Annual Meeting of the Society of Magnetic Resonance. Berkeley, Calif: Society of Magnetic Resonance, 1995; 1960.
15. Bottomley P, inventor. Selective volume method for performing localized NMR spectroscopy. US patent 4,480,228; 1984.
16. Seltzer SE, Getty DJ, Tempany CM, et al. Staging prostate cancer with MR imaging: a combined radiologist-computer system. Radiology 1997; 202:219–226.
17. Yu KK, Scheidler J, Hricak H, et al. Prostate cancer: prediction of extracapsular extension with endorectal MR imaging and three-dimensional proton MR spectroscopic imaging. Radiology 1999; 213: 481–488.
18. Males R, Vigneron D, Nelson S, et al. Addition of MR spectroscopic imaging to MRI significantly improves detection and localization of prostate cancer (abstr). In: Proceedings of the Sixth Meeting of the International Society for Magnetic Resonance in Medicine. Berkeley, Calif: International Society for Magnetic Resonance in Medicine, 1998; 487.
19. Zakian KL, Eberhardt S, Kleinman S, et al. The utility of 1H MRSI in detecting cancer in the prostate transition zone (abstr). In: Proceedings of the 10th Meeting of the International Society for Magnetic Resonance in Medicine. Berkeley, Calif: International Society for Magnetic Resonance in Medicine, 2002; 446.
20. Zakian KL, Eberhardt S, Hricak H, et al. Transition zone prostate cancer: metabolic characteristics at 1H MR spectroscopic imaging—initial results. Radiology 2003; 229:241–247.
21. Sperandeo G, Sperandeo M, Morcaldi M, Caturelli E, Dimitri L, Camagna A. Transrectal ultrasonography for the early diagnosis of adenocarcinoma of the prostate: a new maneuver designed to improve the differentiation of malignant and benign lesions. J Urol 2003; 169:607–610.
22. Neimark AI, Lomshakov AA. Color ultrasonic angiography in evaluation of chronic prostatitis treatment results. Urologiia 2000; 6:21–23.
23. de la Rosette JJ, Giesen RJ, Huynen AL, et al. Automated analysis and interpretation of transrectal ultrasonography images in patients with prostatitis. Eur Urol 1995; 27:47–53.
24. Veneziano S, Pavlica P, Mannini D. Color Doppler ultrasonographic scanning in prostatitis: clinical correlation. Eur Urol 1995; 28:6–9.
25. Wasserman NF. Prostatitis: clinical presentations and transrectal ultrasound findings. Semin Roentgenol 1999; 34:325–337.
26. Gevenois PA, Sintzoff SA Jr, Stallenberg B, et al. Gadolinium-DOTA enhanced MR imaging of prostatic lesions: preliminary results on 14 cases. J Belge Radiol 1992; 75:5–10.
27. Turnbull LW, Buckley DL, Turnbull LS, Liney GP, Knowles AJ. Differentiation of prostatic carcinoma and benign prostatic hyperplasia: correlation between dynamic Gd-DTPA-enhanced MR imaging and histopathology. J Magn Reson Imaging 1999; 9:311–316.
28. Namimoto T, Morishita S, Saitoh R, Kudoh J, Yamashita Y, Takahashi M. The value of dynamic MR imaging for hypointensity lesions of the peripheral zone of the prostate. Comput Med Imaging Graph 1998; 22:239–245.
29. Szolar DH, Ranner G, Preidler KW, Lax S. Non-granulomatous prostatitis: MRI image with endorectal surface coil ("Endo-MRI"). Aktuelle Radiol 1995; 5:67–69.
30. Resnick MI, Kursh ED, Bryan PJ. Magnetic resonance imaging of the prostate. Prog Clin Biol Res 1987; 243(suppl B):89–96.
31. True LD, Berger RE, Rothman I, Ross SO, Krieger JN. Prostate histopathology and the chronic prostatitis/chronic pelvic pain syndrome: a prospective biopsy study. J Urol 1999; 162:2014–2018.
32. Heerschap A, Jager GJ, van der Graaf M, et al. In vivo proton MR spectroscopy reveals altered metabolite content in malignant prostate tissue. Anticancer Res 1997; 17:1455–1460.
33. Kurhanewicz J, Vigneron DB, Nelson SJ, Hricak H. Citrate as an in vivo marker to discriminate prostate cancer from benign prostatic hyperplasia and normal pros-

tate peripheral zone: detection via localized proton spectroscopy. Urology 1995; 45:459–466.
34. Kurhanewicz J, Dahiya R, Macdonald JM, Chang LH, James TL, Narayan P. Citrate alterations in primary and metastatic human prostatic adenocarcinomas: ^{1}H magnetic resonance spectroscopy and biochemical study. Magn Reson Med 1993; 29:149–157.
35. Lowry M, Liney GP, Turnbull LW, Manton DJ, Blackband SJ, Horsman A. Quantification of citrate concentration in the prostate by proton magnetic resonance spectroscopy: zonal and age-related differences. Magn Reson Med 1996; 36:352–358.
36. Liney GP, Turnbull LW, Lowry M, Turnbull LS, Knowles AJ, Horsman A. In vivo quantification of citrate concentration and water T2 relaxation time of the pathologic prostate gland using 1H MRS and MRI. Magn Reson Imaging 1997; 15: 1177–1186.
37. Costello LC, Littleton GK, Franklin RB. Regulation of citrate-related metabolism in normal and neoplastic prostate. In: Sharma RK, Criss WE, eds. Endocrine control in neoplasia. New York, NY: Raven, 1978; 303–314.
38. Costello LC, Franklin RB. Citrate metabolism of normal and malignant prostate epithelial cells. Urology 1997; 50:3–12.
39. Van Dorsten FA, EM, Van Der Graaf M, De La Rosette J, Barentsz J, Heerschap A. Differentiation of prostatitis from prostate carcinoma using 1H MR spectroscopic imaging and dynamic contrast-enhanced MRI (abstr). In: Proceedings of the Ninth Meeting of the International Society for Magnetic Resonance in Medicine. Berkeley, Calif: International Society for Magnetic Resonance in Medicine, 2001; 632.
40. Schiebler ML, Tomaszewski JE, Bezzi M, et al. Prostatic carcinoma and benign prostatic hyperplasia: correlation of high-resolution MR and histopathologic findings. Radiology 1989; 172:131–137.
41. Schiebler ML, Miyamoto KK, White M, Maygarden SJ, Mohler JL. In vitro high resolution 1H-spectroscopy of the human prostate: benign prostatic hyperplasia, normal peripheral zone and adenocarcinoma. Magn Reson Med 1993; 29:285–291.
42. Bennett B, Richardson P, Gardner WJ. Histopathology and cytology of prostatitis. In: Leporand H, Lawson R, eds. Prostate disease. Philadelphia, Pa: Saunders, 1993; 399–413.
43. McNeal J. The prostate gland: morphology and pathobiology. Monogr Urol 1983; 4:5–13.
44. McNeal JE. Normal histology of the prostate. Am J Surg Pathol 1988; 12:619–633.